Simulated Annealing With Variogram-Based Optimization to Quantify Spatial Patterns of Trees Extracted From High-Resolution Images

Vandita Srivastava, Alfred Stein, David G. Rossiter, P. K. Garg, and R. D. Garg

***Abstract*—The recognition of spatial patterns of trees from satellite images is important for forestry, horticulture, and wildlife management. As a spatial optimization problem, we used variogram matching as the objective function for simulated tree arrangements and their simulated reproductions. We developed a variogram difference-based spatial simulated annealing (VDBSSA) method and applied it in reproducing alternate simulated tree arrangements in several orchards in India. Regular, linear, and sparse configurations with clearly separated objects could be distinguished. QuickBird 2 panchromatic images (0.6-m resolution) were binarized, followed by generating simulated images of a similar appearance. The performance of VDBSSA for alternate arrangements with the same spatial structure was explained by pattern characteristics. The density of objects inversely influenced the number of possible alternate arrangements. A sparse configuration gave more choices of alternate spatial arrangements than a dense configuration. VDBSSA is valuable for generating a pattern of well identifiable objects from a remote sensing image.**

***Index Terms*—High spatial resolution satellite imagery, orchard, spatial arrangement, spatial structure, tree distribution pattern, variogram-based simulated annealing (SA).**

I. Introduction

IN FORESTRY and orchard management, the recognition of the spatial pattern of trees is important for the prevention of insect-vectored tree diseases, biomass assessment, forest inventory, and microclimate modeling. Until recently, aerial and field surveys were the only methods to identify individual trees and determine their locations and, hence, their spatial patterns. These methods are expensive and time consuming. Nowadays, high spatial resolution imagery over wide geographic areas is available from Earth satellite remote sensing. This has led to research on computer-based identification and characterization of trees [5]. Once trees are identified, their spatial pattern can be analyzed. The implementation and testing of a similar pattern in another area to achieve a similar productivity or habitat characteristics requires an exact replication of a favorable spatial arrangement. This is not always feasible due to various physical, environmental, and ecological constraints. Thus, other spatial arrangements with a similar interobject spacing and arrangement but different object placement may be required.

A pattern is formed by objects and their relative placement, i.e., their size, shape, and interspacing. For trees of a single species and single age cohort, size and shape vary within well-defined and relatively narrow ranges and thus can be fixed for simplification, whereas intertree spacing may vary according to management decisions and stand history. Intertree spacing is an indicator of health and productivity of trees and growth dynamics of orchards and forests. This motivated our effort to determine tree patterns from imagery and to produce alternate arrangements of trees with a similar spatial structure.

Our procedure consisted of determining a variogram of pixel values in a simulated image of tree objects placed at random locations. This variogram was matched with that of a real image consisting of pre-extracted tree objects. Object boundaries were identified by the transition from tree to nontree. This allowed different arrangements with the same spatial structure. The spatial distribution of trees was a binary random field, i.e., a spatially correlated random process with presence $= 1$ and absence $= 0$ [16]. The observed pattern resulted from deterministic factors such as management activities, climate, and soil variability, combined with a location-specific stochastic component. This stochastic spatial covariance process is assumed to be second order stationary, i.e., there is no difference in expected spatial covariance structure in a forest or orchard with uniform deterministic factors. An empirical model of local spatial autocorrelation is the variogram.

Simulated fields with known characteristics are distinguishable by their variograms (e.g., see [1, Ch. 5]). If a simulated field can be matched to an observed field, then the structure of the observed field can be inferred from that of the simulated field. The question of how to match the two fields and how to find an alternate spatial arrangement with matching variograms

Manuscript received October 20, 2015; revised February 5, 2016 and March 22, 2016; accepted April 1, 2016. Date of publication June 13, 2016; date of current version July 20, 2016. This work was supported in part by the Indian Institute of Remote Sensing, Department of Space, Government of India, and in part by the Faculty of Geoinformation Science and Earth Observation, University of Twente, The Netherlands.

V. Srivastava is with the Indian Institute of Remote Sensing (Indian Space Research Organisation/Department of Space/Government of India), Dehradun 248 001, India (e-mail: vandita@iirs.gov.in).

A. Stein is with the Faculty of Geoinformation Science and Earth Observation, University of Twente, 7522 Enschede, The Netherlands (e-mail: a.stein@utwente.nl).

D. G. Rossiter is with the Section of Soil and Crop Sciences, Cornell University, Ithaca, NY 14850 USA (e-mail: dgr2@cornell.edu).

P. K. Garg is with Uttarakhand Technical University, Government of Uttarakhand, Dehradun 248 007, India, and also with the Indian Institute of Technology Roorkee, Roorkee 247 667, India (e-mail: gargpfce@iitr.ernet.in).

R. D. Garg is with the Department of Civil Engineering, Geomatic Engineering Division, Indian Institute of Technology Roorkee, Roorkee 247 667, India (e-mail: garg_fce@iitr.ac.in).

Color versions of one or more of the figures in this paper are available online at http://ieeexplore.ieee.org.

Digital Object Identifier 10.1109/LGRS.2016.2565743

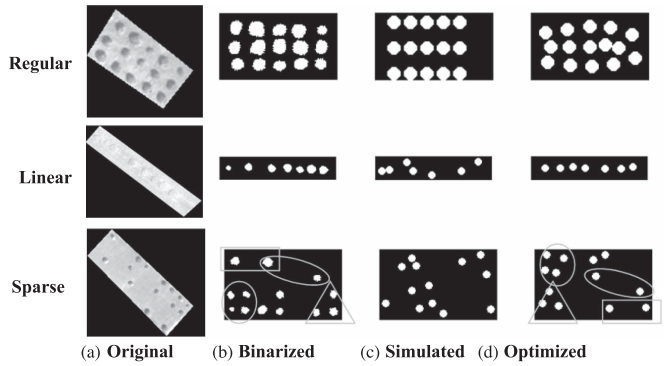

Fig. 1. Four test images: (a) Original image, (b) processed binarized image, (c) simulated image, and (d) image optimized using SA for three (regular, linear, and sparse) tree arrangements. Configurations identified by ellipses are explained in the text.

remains. For this spatial optimization problem, we use simulated annealing (SA) [6], [7]. Spatial SA (SSA) has been applied to optimizing spatial sampling designs [15], random field generation [3], and cluster detection [2] and in satellite-derived information for classification [9] and classification validation [11]. In forestry, it has been used to assess variations in leaf area index assimilation [4], clustering and change detection [12], feature extraction [8], and land allocation [14]. This letter explores the potential of SSA for generating alternate arrangements of trees in an orchard having a matching spatial structure of a given arrangement.

The aim of this study was to explore the potential of SSA to extract alternate patterns of distinct nonoverlapping trees from images by using variogram matching as the optimization function. We considered nonoverlapping tree crowns, as commonly occurring in orchards or parks. Intertree spacing within a restricted range of crown areas was the characterizing variable of the tree distribution pattern. We tested the approach on several images with different characteristics.

II. Images

We used high resolution (61 cm) panchromatic QuickBird 2 imagery. We chose test images from several orchards from around the cities of Dehradun and Saharanpur, northern India. The orchards are dominated by mango (*Mangifera indica*) with $< 15\%$ lychee (*Litchi chinensis*) trees. The size of orchards varies from 0.2 to 25 ha (average of 2 ha), with a density of 50 to 150 trees ha^{-1}. Canopy diameters of managed mango and lychee trees in orchards are of the order of 6–12 m with an average of 8 m. Intertree spacing is of the order of 6–12 m on an average. We chose regular, linear, and sparse tree configurations (see Fig. 1). Simulated images were generated corresponding to the binarized images of the same image size, orientation, and number of circles as trees in the binarized image (see details in Section III).

III. Methodology

The point observations are defined by the original pixels and their values, i.e., using the full spatial and spectral resolution. As we are interested in the presence of the tree crowns, we binarized the image into tree/nontree, resulting in indicator variograms. We retained the full spatial resolution in order to identify tree crown edges. The optimization is a three-step procedure.

- Spectral characteristics like within-object texture, and fuzzy boundaries are removed as these are irrelevant for studying spatial arrangement. After rotating and cropping the image, the Laplacian of Gaussian filter was applied [10], and objects were filled after removing the patch boundary. This resulted in a binary image with a pixel value equal to 1 within a tree object and equal to 0 outside a tree object.
- A synthetic image is generated of the same size as the original image and with the same number of objects. This number is obtained by polygonization, followed by polygon counting, and subtracting one for the boundary polygon.
- The synthetic image is optimized using SA with variogram matching as the optimization function. This is termed "variogram difference-based spatial simulated annealing" (VDBSSA). Variograms of images with similar sizes of trees and similar intertree spacings are likely to match closely. By moving circles in a simulated image until they have the same intertree spacing as in the binarized image, a closely matching variogram is obtained.

VDBSSA is based on SA for finding the global minimum of the objective function [7]. Parameters required by SA are the initial temperature (T_0), the temperature decrement (ΔT), and a stopping criterion. T_0 reflects the initial arrangement of trees, and the temperature T decreases by a cooling schedule defined by ΔT; it also permits small increases in T with a decreasing probability if time evolves. When the stopping criterion is met, the objective function is considered to have reached its minimum, and the trees freeze at the locations thus obtained. These may well show different tree arrangements but still having the same variogram. The objective function (O) is the match between the empirical variograms of the simulated and binarized images. This match is evaluated by the total distance between functions, discretized by the bins. We compared unweighted (1a) and inverse distance weighted separation (1b)

$$O = \sum_{i=1}^{t} \left(V_R(d_i) - V_S(d_i)\right)^2 \tag{1a}$$

$$O = \sum_{i=1}^{t} \left(V_R(d_i) - V_S(d_i)\right)^2 \cdot w_{d_i} \tag{1b}$$

where $V_R(d_i)$ denotes the image variogram value at lag d_i, $V_S(d_i)$ denotes the variogram for the simulated image, d_t is the distance cutoff up to which distances are considered in the optimization function, and w_i is a linearly decreasing weight with increasing lag d_i. Such weights give a higher importance to initial peaks as they are most indicative of tree size and intertree spacing.

T_0 is chosen such that the initial probability of accepting a poorer solution equals a constant (0.8) [1], [6]. T_0 is based on the ratio of average increase in fitness when all inferior

solutions are accepted [6]. The temperature decrement ΔT is a cooling parameter and affects the probability of acceptance of solution

$$P = \frac{Exp(O_n - O_{n-1})}{C} \tag{2}$$

where O_n is the value of the optimization function in the nth iteration (1) and C is an empirical cooling parameter, initialized at T_o that is reduced by a cooling rate equal to 0.0005% of the previous value at successive iterations.

A simulated image of the same size and with the same number of circular objects as of the trees in the observed image was generated using a random placement of circles. A uniformly distributed pseudorandom number generator was used for placing the circle coordinates initially. Circles with a pixel value of 1 were drawn using Bresenham's incremental circle [13] algorithm (modified to plot a solid circle) on a background of pixels with a value of 0. Rotation does not affect the statistics because the tree objects are circular. The radius was the same as the average rounded half of equivalent diameter of trees extracted from the images. Intertree spacing was altered and analyzed as an independent variable. The maximum distance movement of circles during optimization ($D_{\max}$) was fixed as the maximum diagonal distance in the image. $D_{\max}$ was varied by dividing the diagonal distance by the square root of the radii to account for the density of circles for the maximum movement allowed. This $D_{\max}$ was then reduced to $S_{\max}$ in each run using

$$S_{\max} = D_{\max}.e^{\frac{-(i-1)}{h}} \tag{3}$$

where $S_{\max}$ is the maximum shift allowed in the ith iteration and h is an empirical factor that controls the decay. The factor h was decided upon empirically by comparing $D_{\max}$ against iterations by trial and error and was set to 1024. A lower decay factor would lead to a faster decay, and a higher decay factor would lead to a very slow decay with a risk of not covering the complete distance range.

The stopping criterion was defined by the between-iteration change in probability and the maximum number of iterations. Thus, the image was accepted with probability P if either the maximum number of iterations is reached or if the difference in probabilities of the last two consecutive images was less than P_{Th} [see Fig. 1 and (4)]. Its value was set equal to 10^{-6} of the difference in probability values in two consecutive iterations

$$P > 0 \text{ and } P_n - P_{n-1} < P_{Th} \text{ or } n = N_{\max} \tag{4}$$

where n is the current iteration and $N_{\max}$ is the maximum number of iterations. To decide upon $N_{\max}$, the maximum allowed distance for movement in iterations and the temperature were considered. $N_{\max}$ was set so that the minimum possible movement was reached when maximum iterations were reached, starting from $D_{\max}$ in the first iteration, while ensuring that some scope for cooling is left until the last iteration.

One circle of the simulated image was picked randomly and randomly shifted within the limits of $S_{\max}$, and the optimization function was checked. If the movement was rejected, the procedure was repeated until the objective function decreased or the probability was greater than a random number between 0 and 1 as expressed by (2). The procedure was repeated for the next randomly picked circle until (4) was reached.

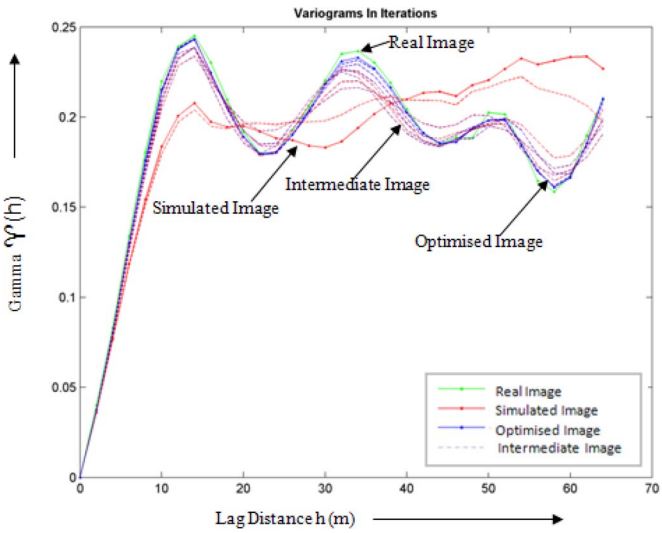

Fig. 2. Behavior of the variogram function during initial, intermediate, and optimized iterations for the regular configuration case.

The numerical precision with which to match the empirical variograms during optimization was decided empirically based upon the actual differences in fitness function at more than 3000 iterations.

The performance of the VDBSSA procedure was assessed by a visual comparison of intertree spacing and patterns of distributions in the binarized and optimized images, produced by the algorithm.

IV. Results

A. Variogram Analysis of the Image With Regular Configuration

The omnidirectional variogram shows a periodic behavior with three cycles and three peaks (see Fig. 2). The first peak shows the maximum semivariance for nearby pixels with different binary values. This corresponds to either the tree diameter, the intertree spacing, or a mixed effect of the two. Intertree spacing is either the inner or outer distance between trees. The mean tree diameter for trees is 12.73 pixels (= 7.64 m). The first peak occurs at about 13 pixels (= 7.8 m) corresponding to the tree diameter (about 7.8 m) or inner tree spacing. The second peak occurs at 36 pixels (= 21.6 m) and may correspond to the outer spacing between two trees. The variogram shows a decreasing semivariance at successive cycles at peaks and valleys and in between as the separation distance between pixels increases, because the number of pixels separated by a particular distance decreases with the increase in separation distance. Thus, the difference in pixel values to calculate the semivariance also decreases with distance.

B. Three Test Cases

Fig. 2 shows the variograms for the regular configuration of trees having nearly equal intertree spacing. The variogram

of the optimized image closely matches the variogram of the binarized image; hence, the optimized image is similar to the binarized image (see Fig. 1). Nontree (black) areas on all four sides of the optimized image closely match the binarized image. The trees in the optimized image have moved closer to each other during optimization to match the spacing of the binarized image. Differences in intertree spacing are likely due to the use of average equivalent diameters in the simulated image, rather than reproducing each tree.

Similar results were observed for the linear configuration of trees. Starting with a random arrangement of circles in the simulated image, the circles in the optimized image have almost completely aligned horizontally and match closely with the arrangement in the binarized image. Optimization has produced a spatial arrangement with a closely matching variogram. The optimized image has almost the same spatial structure but has a slightly different spatial arrangement as that of the binarized image. Spacings between circles in the optimized image closely match those in the binarized image.

Similar results were obtained for the sparse configuration. Here, the circles had more space to move and, thus, more possibilities to produce a matching variogram from the same intertree spacing. Thus, the resultant optimized image differs from the binarized image in its distribution pattern and location of circles. The intertree spacing, however, is close to that in the binarized image. The four geometric shapes in Fig. 1 highlight groups of circles in the optimized image that closely match with those in the binarized image. Their locations are different, but their patterns of distribution and intertree spacings match closely. For example, there is a group of two trees in the optimized image at the right bottom similar to the two trees inside the rectangle at the left top of the binarized image. A similar correspondence is found between circles as highlighted by other three shapes. The fitness function as a function of time for the regular configuration fluctuates, sometimes to an inferior solution, but slowly settles to a minimum value, indicating the close matching of the two variograms. The systematic nonlinear reduction of temperature and maximum distance allowed by $D_{\max}$ shows that the T_0 and initial distance were appropriate. T_0 and ΔT were set so that some scope for cooling remains at the maximum allowed iterations, to still allow image optimization. The maximum allowed distance is also approached, but it does not reach zero as the iteration count approaches its maximum. This choice of T_0 and $D_{\max}$ shows the appropriateness of the chosen stopping criteria, as the temperature did not reach zero even at the final iteration, whereas the distance moved approached its minimum allowed value. A move of a few pixels would allow further refinement but would not significantly affect the results.

The variogram shape changes as it moves from the simulated to the optimized image to closely match the binarized image for the regular configuration.

Weighting proved better than no weighting at 1000 iterations, whereas at 3000 iterations for sparse configuration, no weighting gave slightly better results than weighting. The reason is that, to match the intertree spacing and the distribution pattern, all peaks should equally be matched with no bias to specific distance bins, because of low circle density. This cannot be achieved at a low number of iterations. For the regular and linear configurations, better image matching was obtained using weighting than no weighting even with 3000 iterations. In case of linear and regular configurations, it was more important to focus on initial distance bins due to a higher circle density. Thus, a decreasing weighting of distance bins proved to be superior.

V. Discussion

This letter presents a general method for reproducing the spatial configuration of trees that can be identified as objects in an image. The weighting of the empirical variogram bins affected the optimization. This effect varied with the number of iterations and with different configurations.

Normalizing the diagonal distance of image $D_{\max}$ by the square root of the number of circles influenced the variogram matching. Using this normalized $D_{\max}$ allowed us to also include the circle density which resulted in a higher optimization at a low number of iterations.

Both the number and arrangement of trees in the binarized image influence optimization. As the number of circles increased, the moves required for the simulated image to match the binarized image also increased. In the sparse configuration of trees, the circles had more space to move and, thus, more possibilities of variogram matching with the same intertree spacing in different arrangements of circles. Thus, the resulting optimized image differs from the binarized image in its distribution pattern and location of circles as compared to the linear and regular configuration but does produce the spatial structure. The density of circles affected the success of the optimization. The VDBSSA procedure was more successful in producing a unique spatial arrangement with matching spatial structure in sparse configuration than matching the image in the regular and linear configuration as compared to the sparse configuration. In case of regular and linear configurations, the use of weighting (1b) in the optimization function produced better matching than no weighting. By contrast, for the sparse configuration, no weighting resulted in better image and variogram matching than weighting.

We focused on constant radius circles in the simulated image and variable radius trees in the binarized image. Variograms of the simulated image were able to match that of the binarized image even if there was a difference in intertree spacing in the two images because the image variogram also depended upon the tree size. Retaining the shape of trees in simulated images may result in better matching of intertree spacings with the original binarized image. This may influence the number of alternate arrangements; it is one possible direction for future research.

VI. Conclusion

This letter presented VDBSSA as a method to find alternate distribution patterns with the same spatial covariance structure for clearly separable objects such as trees with nonoverlapping canopies.

VDBSSA successfully produced alternate spatial arrangements by matching binarized and simulated images. In this

way, it inferred the spatially correlated random process from the known simulated image. Differences among alternate configurations depended mostly on the density of the original configuration. A future challenge will be to extend it from clearly separated circular trees to more realistic tree shapes in a simulated image, to nonbinarized images, and to trees with overlapping crowns. The use of directional variograms and fitting of variogram models instead of the original empirical variogram during SSA could be explored. Another possibility is to explore multipoint statistics in matching the binarized and simulated images.

VDBSSA can be generalized from individual trees to patches of trees, agricultural crops, and forested landscapes for producing scenes with different arrangements with similar spatial structure. Possibly, it could be extended from circular to other shapes of separated objects such as buildings or lakes that occur at different scales.

The method can be useful as well in studies on forests, precision agriculture, and horticulture, where intertree or interplant spacing influences growth, competition, health, quality, and productivity and is a factor in selecting treatments for disease or malformation. By obtaining several images of similar distribution configurations, optimal treatments for all similar configurations can be identified. This has a potential application in designing alternative planting schemes. VDBSSA can be applied to obtain those, e.g., starting with designs that have proven good characteristics. Such spatial arrangements with matching spatial structure can be used for image matching, i.e., to find images displaying clusters of similarly configured objects. This is promising in content-based image retrieval for the retrieval of images based on object distribution using their shape and size and interobject spacing. An important case is the interpretation of dominant tree size, spacing, and arrangement. Such information, once obtained, can be used to appropriately detect trees. A sparse configuration of individual trees, for example, requires a different extraction than a dense configuration of partly overlapping trees. VDBSSA thus has potential applications in agricultural design and planning practices, e.g., in suggesting alternative designs for the distribution of facilities or resources of a polygon type. Finally, it can be applied in virtual reality to design artificial landscapes with known characteristics.

REFERENCES

[1] D. J. Brus and G. B. M. Heuvelink, "Optimization of sample patterns for universal kriging of environmental variables," *Geoderma*, vol. 138, pp. 86–95, 2007.
[2] B. Chen *et al.*, "Even sampling designs generation by efficient spatial simulated annealing," *Math. Comput. Model.*, vol. 58, pp. 670–676, 2011.
[3] C. V. Deutsch and A. G. Journel, *Geostatistical Software Library and User's Guide*. London, U.K.: Oxford Univ. Press, 1992.
[4] Y. Dong *et al.*, "Integrating a very fast simulated annealing optimization algorithm for crop leaf area index variational assimilation," *Math. Comput. Model.*, vol. 58, no. 3/4, pp. 877–885, Aug. 2013.
[5] P. Gong *et al.*, "Photo-ecometrics for forest inventory," *Geograph. Inf. Sci.*, vol. 5, pp. 9–14, 1999.
[6] S. Kirkpatrick, "Optimization by simulated annealing: Quantitative studies," *J. Statist. Phys.*, vol. 34, no. 5, pp. 975–986, Mar. 1984.
[7] S. Kirkpatrick, C. D. Gelatt, and M. P. Vecchi, "Optimization by simulated annealing," *Science*, vol. 220, pp. 671–680, 1983.
[8] C. Lacoste, X. Descombes, and J. Zerubia, "Unsupervised line network extraction in remote sensing using a polyline process," *Pattern Recognit.*, vol. 43, no. 4, pp. 1631–1641, Apr. 2010.
[9] S. Le Hégarat-Mascle, D. Vidal-Madjar, and P. Olivier, "Applications of simulated annealing to SAR image clustering and classification problems," *Int. J. Remote Sens.*, vol. 17, no. 9, pp. 1761–1776, 1996.
[10] D. Marr and E. Hildreth, "Theory of edge detection," *Proc. Roy. Soc. London B, Biol. Sci.*, vol. 207, pp. 187–217, 1980.
[11] C. Miravet and F. B. Rodríguez, "A two-step neural-network based algorithm for fast image super-resolution," *Image Vis. Comput.*, vol. 25, no. 9, pp. 1449–1473, Sep. 2007.
[12] N. S. Mishra, S. Ghosh, and A. Ghosh, "Fuzzy clustering algorithms incorporating local information for change detection in remotely sensed images," *Appl. Soft Comput.*, vol. 12, no. 8, pp. 2683–2692, Aug. 2012.
[13] D. F. Rogers, *Procedural Elements for Computer Graphics*. New York, NY, USA: McGraw-Hill, 1984.
[14] I. Santé-Riveira, M. Boullón-Magán, R. Crecente-Maseda, and D. Miranda-Barrós, "Algorithm based on simulated annealing for land-use allocation," *Comput. Geosci.*, vol. 34, no. 3, pp. 259–268, Mar. 2008.
[15] J. W. Van Groenigen, W. Siderius, and A. Stein, "Constrained optimisation of soil sampling for minimisation of the kriging variance," *Geoderma*, vol. 87, no. 3/4, pp. 239–259, Jan. 1999.
[16] R. Webster and M. A. Oliver, *Geostatistics for Environmental Scientists*. Chichester, U.K.: Wiley, 2007.